Mesozoic 001 (3): 349–365
https://www.mapress.com/mz/

Article

ISSN 3021-1859 (print edition)
MESOZOIC
ISSN 3021-1867 (online edition)

https://doi.org/10.11646/mesozoic.1.3.15
http://zoobank.org/urn:lsid:zoobank.org:pub:A35BE2C7-D955-44FF-9132-1CB63CC7B0D9

The fate of the Xigaze forearc basin after Late Cretaceous filling (South Tibet)

JING-XIN JIANG[1, *], XIU-MIAN HU[1], EDUARDO GARZANTI[2], MARCELLE BOUDAGHER-FADEL[3] & WEI AN[1, 4]

[1]*State Key Laboratory of Mineral Deposit Research, School of Earth Sciences and Engineering, Nanjing University, Nanjing 210023, China*
[2]*Laboratory for Provenance Studies, Department of Earth and Environmental Sciences, Università di Milano-Bicocca, Milano 20126, Italy*
[3]*Department of Earth Sciences, University College London, London WC1H0BT, UK*
[4]*School of Resources and Environmental Engineering, Hefei University of Technology, Hefei 230009, China*
jjxcug24@163.com; https://orcid.org/0009-0004-2217-2118
huxm@nju.edu.cn; https://orcid.org/0000-0002-5401-8682
eduardo.garzanti@unimib.it; https://orcid.org/0000-0002-8638-9322
m.fadel@ucl.ac.uk; https://orcid.org/0000-0002-2339-2444
anwei@hfut.edu.cn; https://orcid.org/0000-0001-5799-9394
**Corresponding author*

Abstract

The Xigaze forearc basin is a key region to understand the evolution of active continental margins related to Neo-Tethyan oceanic subduction. Most studies have focused on the sedimentary evolution during filling of the marine basin, but we here provide a detailed sedimentological and biostratigraphic analysis of the last, uppermost Cretaceous to Paleogene phases of forearc sedimentation documented by the shallow marine to deltaic to fluvial Qubeiya, Quxia, and Jialazi formations exposed in the Cuojiangding area. By comparing these sequences with regional tectonic and global climate events and sea-level curves, a reconstruction of the environmental evolution during this final filling stage is proposed, placing emphasis on the eustatic control of carbonate deposition in the Qubeiya and Jialazi formations. These transgressive intervals are separated by two regressive episodes unrelated to global sea-level trends that led to the demise of the carbonate platform. The first episode, documented by fan-delta deposits of the Quxia Formation, occurred at the time of initial India-Asia collision. The second episode, documented in the central part of the Jialazi Formation, occurred during the Paleocene-Eocene Thermal Maximum, likely driven by an intensified hydrological cycle. These results provide new insight into the palaeo-tectonic and palaeo-environmental evolution during the closure of the Neotethys seaway between India and Asia.

Keywords: Xigaze forearc basin, depositional environment, microfacies analysis, biostratigraphy, South Tibet

Introduction

Forearc basins, located between the magmatic arc and the accretionary wedge in arc-trench systems, are generally affected indirectly by oceanic subduction-related magmatic and tectonic processes. As a consequence, they preserve the complete sedimentary record during the cycle from subduction initiation to collision, essential to understand the evolution of active continental margins (Ingersoll, 1979; Einsele *et al*., 1994; Dickinson, 1995; DeGraaff-Surpless *et al*., 2002; Cawood, 2005; An *et al*., 2014; Orme *et al*., 2015). The Xigaze forearc basin, situated along the southern margin of the Lhasa Block by the northward subduction of the Neotethys Ocean (Wang *et al*., 2017). After an initial starved stage documented by slow accumulation of chert layers, the basin served as the primary depositional area for detritus eroded from the Gangdese arc, providing a direct record of the tectonic and palaeogeographic evolution of the southern margin of Asia (Garzanti *et al*., 1987; Garzanti & Van Haver, 1988; Einsele *et al*., 1994; Wu *et al*., 2010; Wang *et al*., 2012; An *et al*., 2014).

After decades of extensive stratigraphic, sedimentary provenance and tectonic research, a comprehensive understanding of the geological evolution of the Xigaze forearc basin has been achieved. However, most studies have primarily focused on the lower and central part of the basin-filling megasequence, represented by deep-

Submitted: 19 Sept. 2024; accepted by D.-Y. Huang: 26 Sept. 2024; published: 27 Sept. 2024

water turbidites transitioning upward to deltaic deposits, with limited attention given to the younger strata (Qian *et al*., 1982; Liu *et al*., 1988; Sun & Wang, 2001; Wan *et al*., 2001; Li *et al*., 2008; An *et al*., 2014; Orme *et al*., 2015; Hu *et al*., 2016b; Wang *et al*., 2017; Ingalls, 2019). Continuously exposed in the Cuojiangding area of southern Tibet is the most complete uppermost Cretaceous to Paleogene succession of the Xigaze forearc basin, offering an excellent record of the sedimentary and palaeogeographic evolution of the southern active margin of Asia during this time interval (Qian *et al*., 1982; Liu *et al*., 1988; Hu *et al*., 2016b). The aim of the present study is to systematically investigate the uppermost Cretaceous–Paleogene stratigraphic units of the Xigaze forearc basin and relate the observed changes in sedimentary facies to potential controlling factors including tectonics, climate, and eustatism. This approach aims to provide new insights into the palaeogeodynamic evolution of the southern active margin of Asia during the progressive closure of the Neotethys Ocean, both prior to and during the India-Asia collision.

Geological setting

The Xigaze forearc basin

The Xigaze forearc basin is bordered by the Yarlung-Zangbo ophiolite belt to the south and by the Gangdese arc to the north and extends for ~550 km east-west along the suture zone with a width of ~25 km (Fig. 1A). The basin was filled by Albian to Santonian deep-sea turbidites (Einsele *et al*., 1994; Dürr, 1996; Wan *et al*., 1998; Wang *et al*., 1999, 2012), overlain by Campanian-Maastrichtian shelfal and deltaic deposits (Liu *et al*., 1988; Wang *et al*., 2012; An *et al*., 2014; Hu *et al*., 2016b), followed in turn by fluvial sediments marking the final filling stage. After the early Paleogene India-Asia collision onset (DeCelles *et al*., 2014; Ding *et al*., 2016 Hu *et al*., 2015, 2016a), the Xigaze forearc basin evolved into a syn-collisional basin (Orme *et al*., 2015; Hu *et al*., 2016b).

Stratigraphy of the Cuojiangding area

In the studied Cuojiangding area (Zhongba County, southern Tibet), belonging to the western segment of the Xigaze forearc basin, well-preserved shallow-marine and continental strata of the Qubeiya, Quxia, and Jialazi formations (Qian *et al*., 1982; Liu *et al*., 1988) document the terminal evolution of the basin (Ding *et al*., 2005; Hu *et al*., 2016b). The stratigraphic succession is exposed in a syncline, with strata on its flanks being in tectonic contact along the Gangdese thrust in the north and with the Zhongba ophiolite belt in the south (Fig. 1B).

The Qubeiya Formation, ~310-m-thick in the Goukou section where it conformably overlies the Upper Cretaceous Padana Formation (Fig. 2C), mainly consists of light gray to grayish-yellow marlstone, with thin layers of calcareous sandstone interbedded in the middle and lower parts (Fig. 2E). Abundant benthic foraminifers are locally associated with bivalves, gastropods, and crinoid remains (Fig. 2F, G). A Campanian to Maastrichtian age is indicated by ammonoid and foraminiferal assemblages (Liu *et al*., 1988; Sun & Wang, 2001; Wan *et al*., 2001; Hu *et al*., 2016b).

The 110–120 m-thick Quxia Formation conformably overlies with transitional contact with the Qubeiya Formation (Fig. 2D). The lower member is dominated by gray-green and purplish-red mudrock with interbedded medium-thick sandstone layers displaying erosional basal surfaces and oblique lamination. The upper member is characterized by multiple conglomerate-sandstone-mudrock cyclothems (Fig. 2I) with imbricated structures in conglomerates (Fig. 2J) and oblique lamination in sandstones. A maximum depositional age of 66 Ma (Cretaceous/Tertiary boundary) is indicated by detrital-zircon chronostratigraphy (Hu *et al*., 2016b).

The ~200-m-thick Jialazi Formation conformably overlies the Quxia Formation and chiefly consists of limestone with abundant benthic foraminifers, bivalves, gastropods, echinoderms, corals and coralline algae, interbedded with mudrock and sandstone (Fig. 2K–M). Foraminiferal biostratigraphy indicates a Late Paleocene to early Eocene age (Liu *et al*., 1988; Wan *et al*., 2001; Hu *et al*., 2016b; Jiang *et al*., 2021). Several tuff layers in the middle Jialazi Formation yielded Ar-Ar ages of 56.3 ± 2.1 Ma (Ding *et al*., 2005) and zircon U-Pb ages from 54.9 to 55.7 Ma (LA-ICP-MS; Hu *et al*., 2016b) or from 55.1 to 56.1 Ma (SIMS; Jiang *et al*., 2021). The youngest cluster of detrital-zircon ages constrains the top of the formation to the earliest Eocene (54 ± 1 Ma; Hu *et al*., 2016b). Carbonate stratigraphy was redefined by Kahsnitz *et al*. (2017). Jiang *et al*. (2021) identified the Paleocene Eocene Thermal Maximum (PETM) record in the Jialazi Formation and reconstructed the sedimentary and hydrological-cycle evolution during this hyperthermal event based on carbon-isotope stratigraphy, biostratigraphy, and chronostratigraphy.

Material and methods

Two stratigraphic sections were measured: the Goukou section exposing the Qubeiya, Quxia and lower Jialazi formations (29°55'45.90" N, 84°19'14.70" E; Fig. 2A), and the Quxia B section chiefly exposing the Quxia and

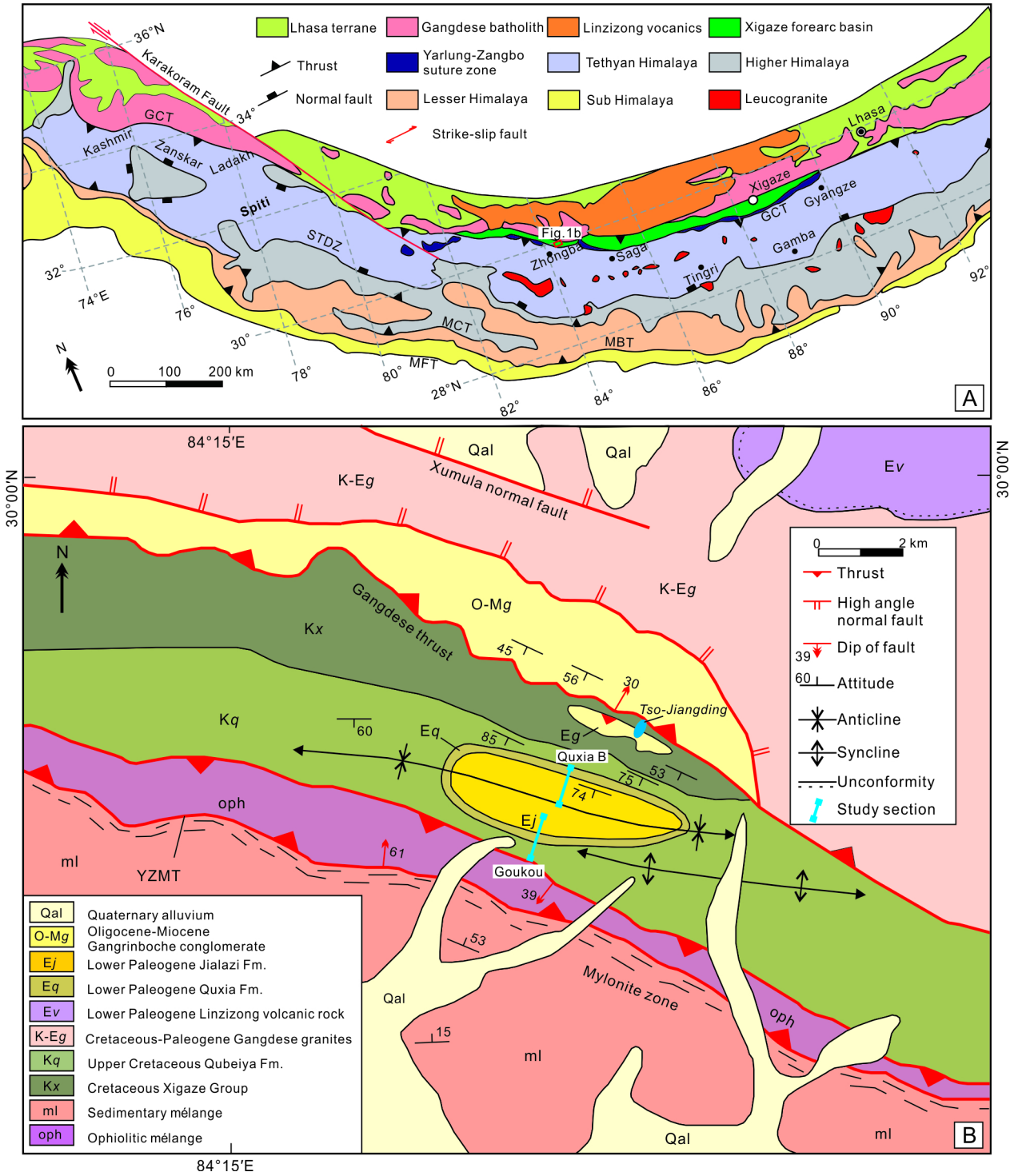

FIGURE 1. Geological maps. **A**, Simplified tectonic map of Himalayan belt and southern Tibet (redrawn from Hu *et al*., 2016b), illustrating major structural features: Great Counter Thrust (GCT), South Tibetan Detachment Zone (STDZ), Main Central Thrust (MCT), Main Boundary Thrust (MBT), Main Frontal Thrust (MFT). **B**, Geological map of Cuojiangding area (redrawn from Ding *et al*., 2005) showing location of studied Goukou and Quxia B sections.

Jialazi formations (29°56'19.20" N, 84°19'32.10" E; Fig. 2B); 371 samples were collected in the Goukou section and 79 samples from the Quxia B section. Carbonate samples were collected at 1-meter intervals and sandstone was sampled at the main lithological changes. This study focuses principally on the environmental evolution testified by the Qubeiya and Quxia formations and integrates the detailed description of the Jialazi Formation in Jiang *et al*. (2021) to obtain further information on the final stage and demise of seaways from the Xigaze forearc basin.

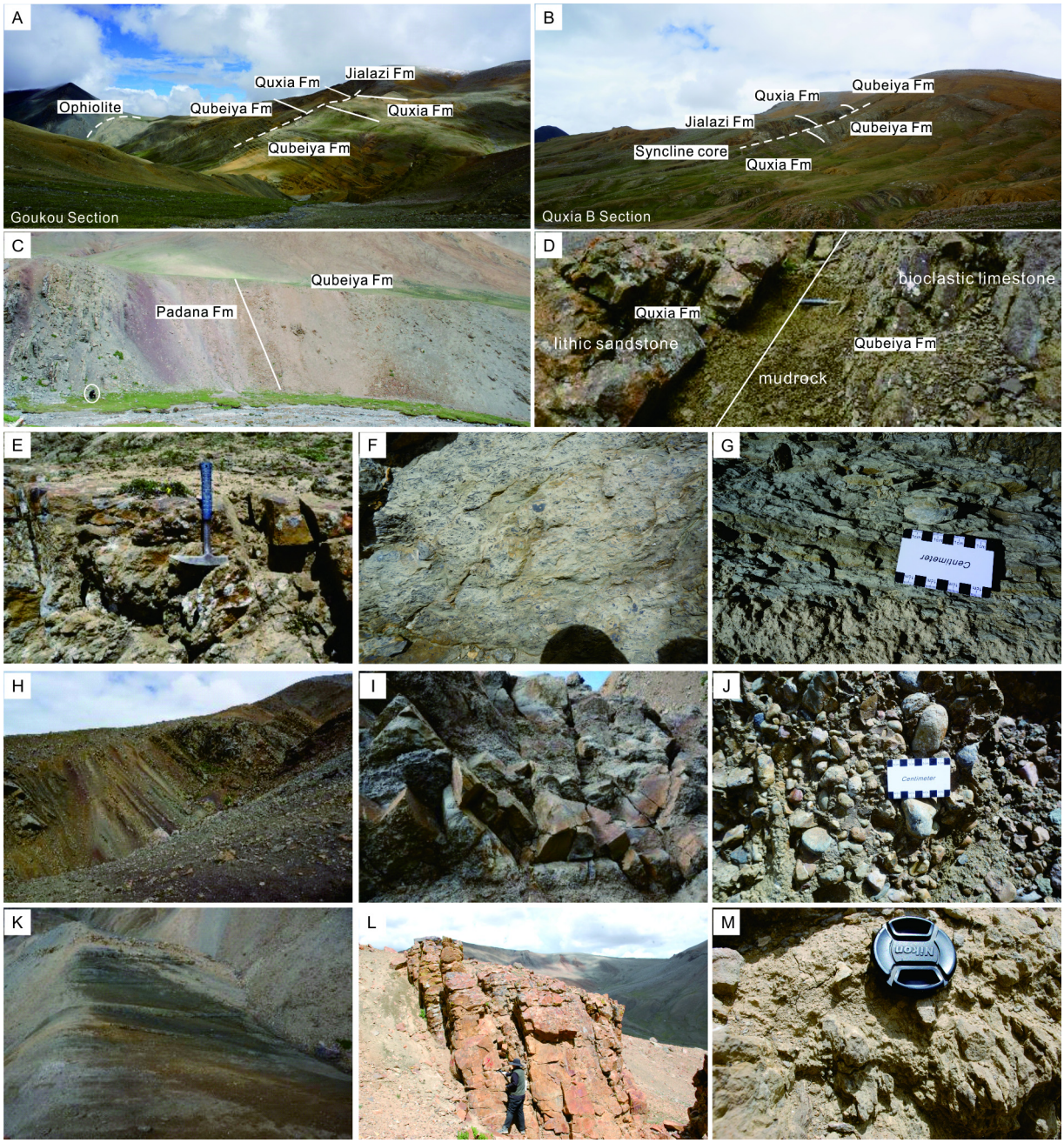

FIGURE 2. Field photographs. **A**, **B**, Full view of measured Goukou and Quxia B sections. **C**, Conformable boundary between Padana and Qubeiya formations. **D**, Transitional contact between Qubeiya and Quxia formations. **E**, Calcareous sandstone in lower Qubeiya Formation. **F**, Abundant benthic foraminifers in marlstone of Qubeiya Formation. **G**, Bivalves in marlstone of Qubeiya Formation. **H**, Greenish and reddish mudrock intercalated with sandstone in lower Quxia Formation. **I**, Conglomerate-sandstone-mudrock cyclothems in upper Quxia Formation. **J**, Rounded and poorly sorted pebbles in upper Quxia Formation. **K**, Greyish mudrock intercalated with bioclastic limestone in lower Jialazi Formation. **L**, Medium to thick-bedded sandstone in middle Jialazi Formation. **M**, Coral colony in lower Jialazi Formation.

Biostratigraphy

A detailed biostratigraphic description of the uppermost Cretaceous to lower Paleogene shallow-marine successions of southern Tibet, resulting in a new comprehensive scheme based on shallow benthic foraminiferal zones (SBZ) of Serra-Kiel (1988), was provided by BouDagher-Fadel *et al*. (2015, 2018). In the present study, a systematic analysis of benthic foraminifera in carbonate strata of the Qubeiya and Jialazi formations was conducted following the same criteria, using oriented thin sections.

Facies analysis

Descriptions are based on Dunham (1962; revised and integrated by Embry & Klovan, 1971) for carbonate

rocks (siliciclastic detritus <10%), on Mount (1985) for mixed carbonate-siliciclastic sediments (siliciclastic detritus >10%), and on lithofacies (LF) for siliciclastic rocks. Microfacies (MF) analysis was based on texture, sedimentary structure, grain composition, and fossil content. Interpretations considered lithological characteristics observed in both thin sections and outcrops, standard carbonate microfacies and depositional models of Flügel (2010), and ecological models of benthic foraminifera by Beavington-Penney and Racey (2004).

Results

Larger benthic foraminiferal (LBF) biostratigraphy

The distribution of diagnostic species of benthic foraminifera in the Qubeiya and Jialazi formations is illustrated in figures 3 and 4.

The Qubeiya Formation is characterized by benthic foraminifera *Lepidorbitoides* (*L. blanfordi*, *L. minor*, and *L.* sp. C) and *Orbitoides* (Fig. 3A–E), spanning the TLK2 and TLK3 biozones corresponding to Maastrichtian 2 and Maastrichtian 3. The TLK2/TLK3 boundary is defined by the continuous occurrence of *Lepidorbitoides* sp. A, first appearing in sample 17CJD13 but being continuously present from sample 17CJD172 on. The *Omphalocyclus macroporus-Abathomphalus mayaroensis* assemblage appears in sample 17CJD130 but its occurrence is sporadic through the section. *Lepidorbitoides socialis* appears near the base of the section (17CJD21) and continues to the top of TLK3. *Orbitoides* sp. A is found only at the base of the section, *Lepidorbitoides* sp. D, *L.* sp. F, *Orbitoides media*, *O.* sp. B, *O. faujasii*, and *Pseudotextularia punctulata* mostly in TLK2, and *L.* sp. E and *O. medius* commonly in TLK2 but sporadically in TLK3.

The TLK3/TP1 boundary, TP1 (SBZ1-SBZ2) and the lower part of TP2 (lower SBZ3) are not biostratigraphically documented in the Cuojiangding area, and only the fossil record of the upper part of TP2 to TP5 (upper SBZ3-SBZ6) is documented in the Jialazi Formation. The lower part of the Jialazi Formation is dominated by the *Miscellanea-Daviesina-Ranikothalia* assemblage (Fig. 3F–H), corresponding to the late Thanetian (upper SBZ3 to lower SBZ5; Jiang *et al*., 2021). The upper part of the Jialazi Formation is characterized instead by the *Assilina-Nummulites-Discocyclina* assemblage (Fig. 3I–M), corresponding to the early Ypresian (upper SBZ5 to early SBZ6). The intervening unfossiliferous middle part of the Jialazi Formation is constrained within SBZ5 based on fossil assemblages from the underlying and overlying strata.

Facies description and interpretation

Overall, eleven carbonate microfacies (MF) and four clastic lithofacies (LF) were identified. They are described below, formation by formation, in stratigraphic order and according to their inferred relative positions from land to open sea (Figs 5–7).

Qubeiya Formation

1. MF2 Sandy *Lepidorbitoides* wackestone

MF2 is represented in marlstone interbedded with calcareous sandstone at the base of the Qubeiya Formation. Bioclasts are predominantly *Lepidorbitoides* and *Orbitoides* (10–15% of the rock) mostly appearing as well-preserved elongated shapes and locally associated with bivalve and echinoderm remains. The matrix (75–80% of the rock) consists of micrite, microspar, and terrigenous silt; bioturbation is visible (Fig. 5A–C). The limited biodiversity and occurrence of siliciclastic detritus indicate a restricted environment close to land; elongated foraminifera suggest weak depositional hydrodynamics and relatively deep water. MF2 is thus inferred to document a deep lagoon connected to land and relatively isolated from the open ocean.

2. MF3 *Lepidorbitoides*-bearing silty mudstone

MF3 is represented in silty mudstone alternating with MF2 at the base of the Qubeiya Formation. Micrite and silt constitute 90% of the rock, with sporadic *Lepidorbitoides*, *Orbitoides*, or rare echinoderm fragments. Bioturbation occurs (Fig. 5D–F). Fossils are similar as in MF2 but smaller and with cleaner shells, indicating that MF3 formed in clearer waters with less clastic input, plausibly closer to the center of the lagoon.

3. MF4 *Lepidorbitoides* floatstone

MF4 is represented in the middle to upper Qubeiya Formation. Bioclasts are predominantly *Lepidorbitoides* and *Orbitoides* (mainly 15–25%, but up to 40% of the rock), mostly well-preserved, with oval and elongated shapes with >2 mm average size. Echinoderm fragments, bivalves, bryozoans, and planktonic foraminifera (~5%) occur. The matrix is micrite with minor silt (Fig. 5G–I). As in MF2 and MF3, fossil assemblages in MF4 are characterized by *Lepidorbitoides*, but with more diversified bioclasts associated with larger benthic foraminifera commonly found aligned or in clusters, suggesting hydrodynamic transport. MF4 is inferred to reflect frequent storm activity during a period of warmer ocean waters, in an open marine environment above storm wave base.

4. Summary

The Qubeiya Formation is characterized by widespread *Lepidorbitoides*, thriving at intermediate to low latitudes in shelfal to lagoonal environments with water depths ≤ 40 m (Geel, 2000; Beavington-Penney & Racey, 2004; Flügel, 2010; Malarkodi *et al*., 2017). Unlike

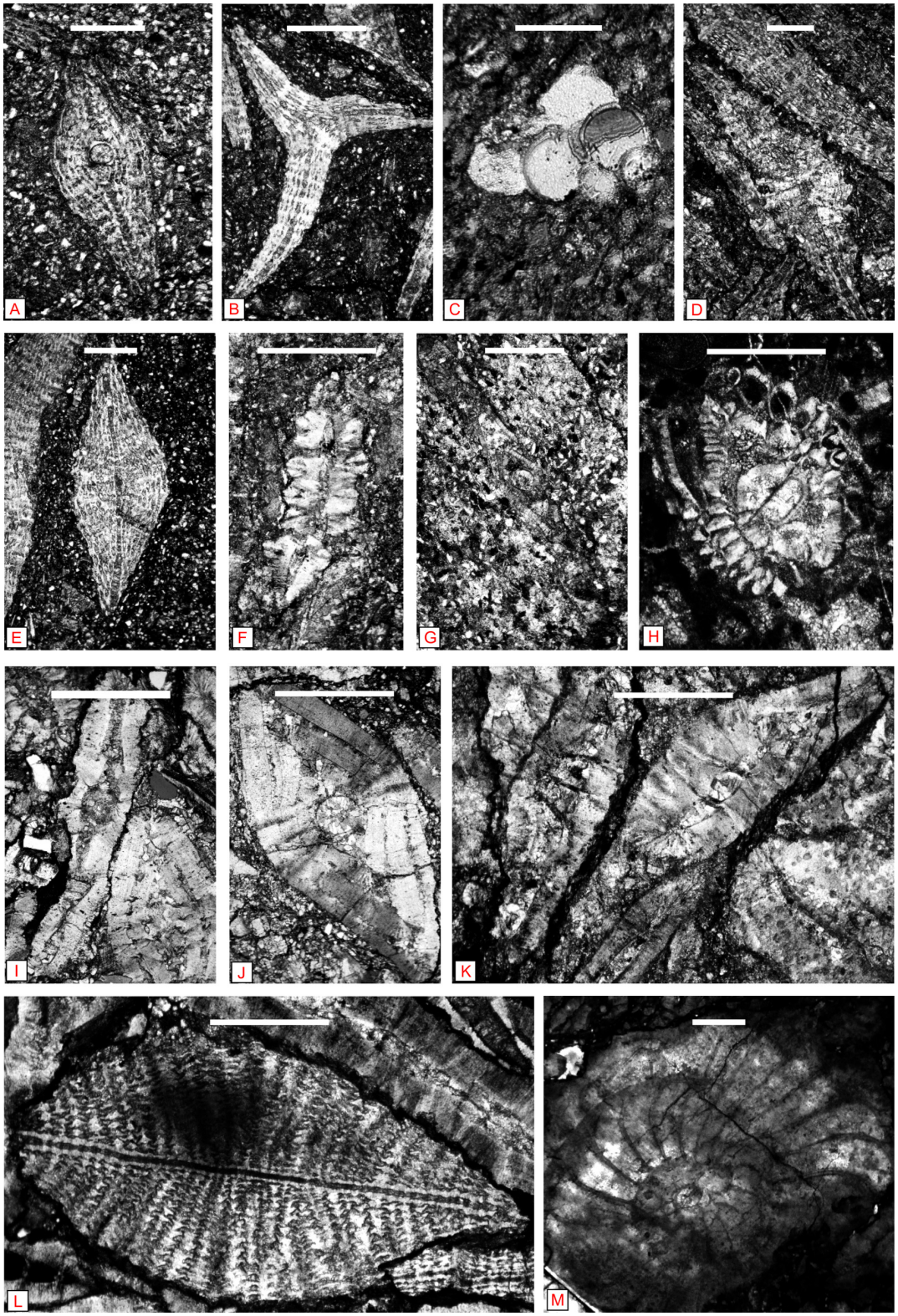

FIGURE 3. Benthic foraminifera from Goukou and Quxia B sections. **A**, *Lepidorbitoides blanfordi* Rao, Maastrichtian 2, TLK2. **B**, *L.* sp. F, Maastrichtian 2. TLK2. **C**, *Pseudotextularia punctulata* (Cushman), Maastrichtian 2. TLK2. **D**, *L.* sp. A, Maastrichtian 3, TLK3. **E**, *L. minor* (Schlumberger), Maastrichtian 3, TLK3. **F**, *Assilina subspinosa* Davies, early to middle Thanetian, TP2-TP3 (SBZ3-4). **G**, *Ranikothalia sindensis* (Davies), middle to late Thanetian, TP3-TP4 (SBZ4). **H**, *Miscellanea miscella* (d'archiac and Haime), late Thanetian, TP4 (SBZ4-5). **I**, *Ranikothalia sindensis* (recycled); *Nummulites globulus* Leymerie, earliest Ypresian, TP5 (SBZ6). **J**, *Nummulites globulus* Leymerie, earliest Ypresian, TP5 (SBZ6). **K**, *Daviesina ruida* (Schwager), earliest Ypresian, TP5 (SBZ6). **L**, *Assilina leymeriei* (d'Archiac and Haime), *Discocyclina dispansa* (Sowerby), earliest Ypresian, TP5 (SBZ6). **M**, *Daviesina salsa* (Davies and Pinfold), earliest Ypresian, TP5 (SBZ6). Scale bars: **A**, **B**, **D**–**F**, **I**–**M** = 1 mm; **C**= 0.25 mm; **G**, **H** = 0.5 mm.

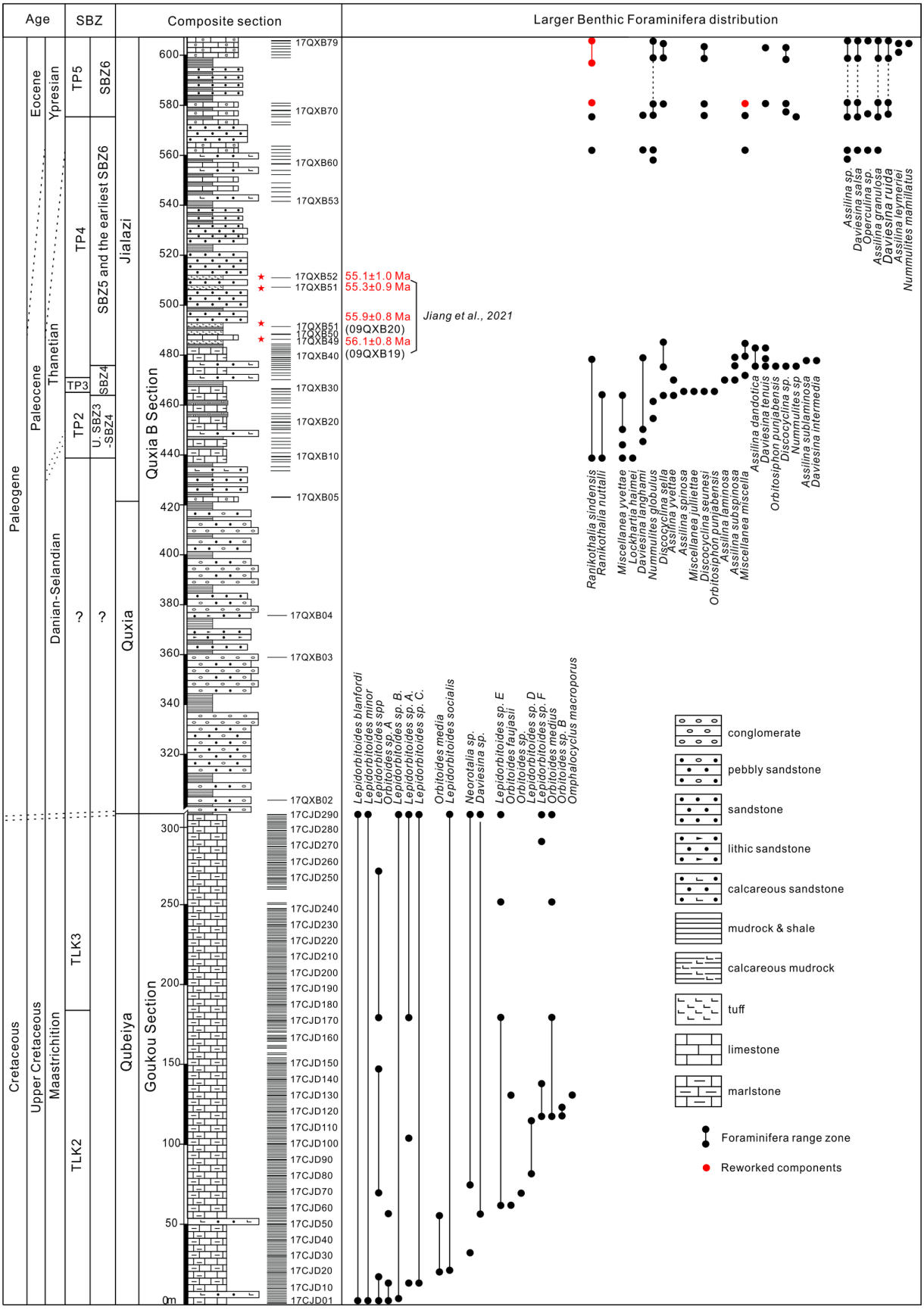

FIGURE 4. Stratigraphic distribution of larger benthic foraminifers in Cuojiangding succession (Qubeiya Fm. in Goukou Section; Quxia and Jialazi Fms. in Quxia B Section). SIMS ages of zircon in tuff (Jiang *et al*., 2021) are indicated in red. SBZ: Shallow marine benthic-foraminifera zone; TLK: Tibetan Late Cretaceous foraminiferal biozones; TP: Tibetan Paleogene foraminiferal biozones.

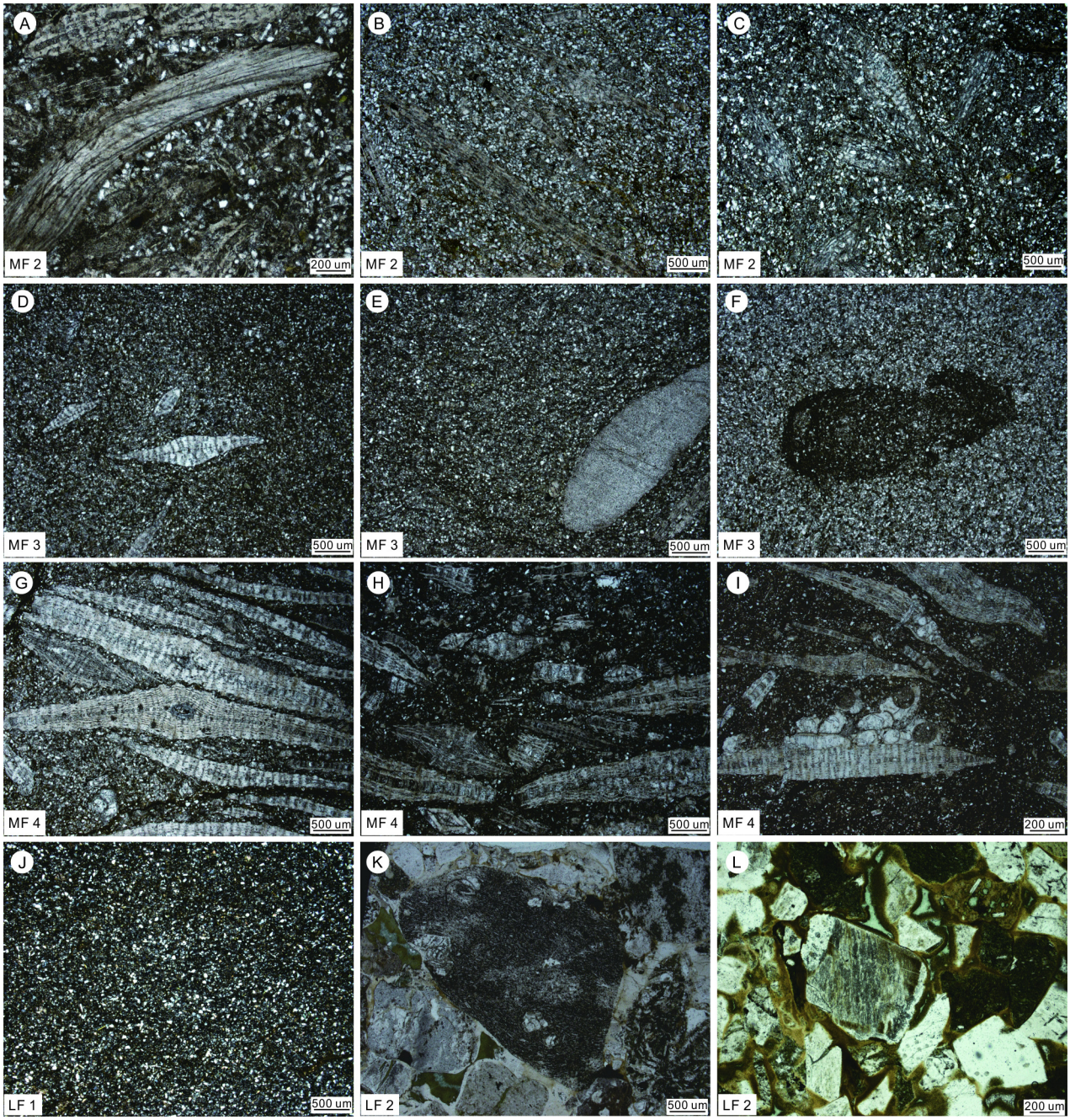

FIGURE 5. Representative microfacies of Qubeiya and Quxia formations. **A**–**C**, MF2 sandy *Lepidorbitoides* wackestone. **D**–**F**, MF3 *Lepidorbitoides*-bearing silty mudstone. **G**–**I**, MF4 *Lepidorbitoides* floatstone. **J**, LF1 fine sandstone. (**K**, **L**,) LF2 litho-feldspathic sandstone.

other euryhaline marine organisms, *Lepidorbitoides* is tolerant of terrigenous pollution (Robles-Salcedo *et al*., 2013). MF2 and MF3 contain more terrigenous detritus and a more limited biota, indicating a more restricted lagoonal environment closer to land than MF4, which is characterized by storm deposits with a diversified biota indicating a more open marine environment. The Qubeiya Formation that overlies the deltaic Padana Formation is thus inferred to have been deposited in shallow open marine to lagoonal environments during transgression.

Quxia Formation

1. LF1 Mudrock with sandstone

LF1 is represented in the lower Quxia Formation, in sequences of gray-green and purplish-red mudrock with locally intercalated black claystone, siltstone, or medium-bedded fine to locally coarse sandstone showing basal erosional surfaces and oblique lamination (Figs 2H, 5J). Lithology and sedimentary structures indicate a floodplain environment with overbank and channel deposits (Miall, 2013). Semiarid climate is suggested by purplish-red and gray-green hues of mudrock.

2. LF2 Conglomerate-sandstone-claystone cyclothems

LF2 is represented in fining-upward cyclothems of the middle and upper Quxia Formation, dominated by matrix-supported conglomerate with silt to coarse-sand matrix (Fig. 2I, J). Pebbles range 2–5 cm in size on average, but cobbles up to 15–20 cm displaying imbricate structures occur. Poorly sorted and commonly well-rounded clasts are mainly intermediate to felsic igneous rocks (andesite, rhyolite, granite), chert, and sandstone; limestone clasts were not observed (Fig. 5K, L). Sandstone beds with moderate to poor lateral continuity display basal erosional surfaces and oblique lamination; inverse grading and lenses of coarse sandstone within conglomerates are present (Fig. 5I, J). Such coarse-grained sediments were deposited as debris flows in a fan-delta environment (McPherson *et al*., 1987; Miall, 2013).

Jialazi Formation

Two clastic lithofacies and eight carbonate facies were identified, allowing us to define four main depositional settings (Figs 6, 7).

1. Fan-delta front

LF3 (claystone with sandstone and limestone) and LF4 (massive sandstone and claystone) indicate a fan-delta front environment. LF3, occurring in the basal and upper parts of the Jialazi Formation, is characterized by gray-black mudrock interbedded with thin to medium layers of medium to fine sandstone (Figs 2K, 6I), indicating a delta front environment (Miall, 2013). Widespread mudrock represent distal bottomset beds, whereas laterally continuous, laminated sandstone layers with uniform thickness indicate sheet-sand deposition on the delta front.

LF4 consists of thick to very thick-bedded sandstone and pebbly sandstone interbedded with thin layers of siltstone and mudrock in the middle Jialazi Formation (Figs 2L, 6J). Sandstone layers can exceed 1 m in thickness and lack distinct sedimentary structures. Interbedded

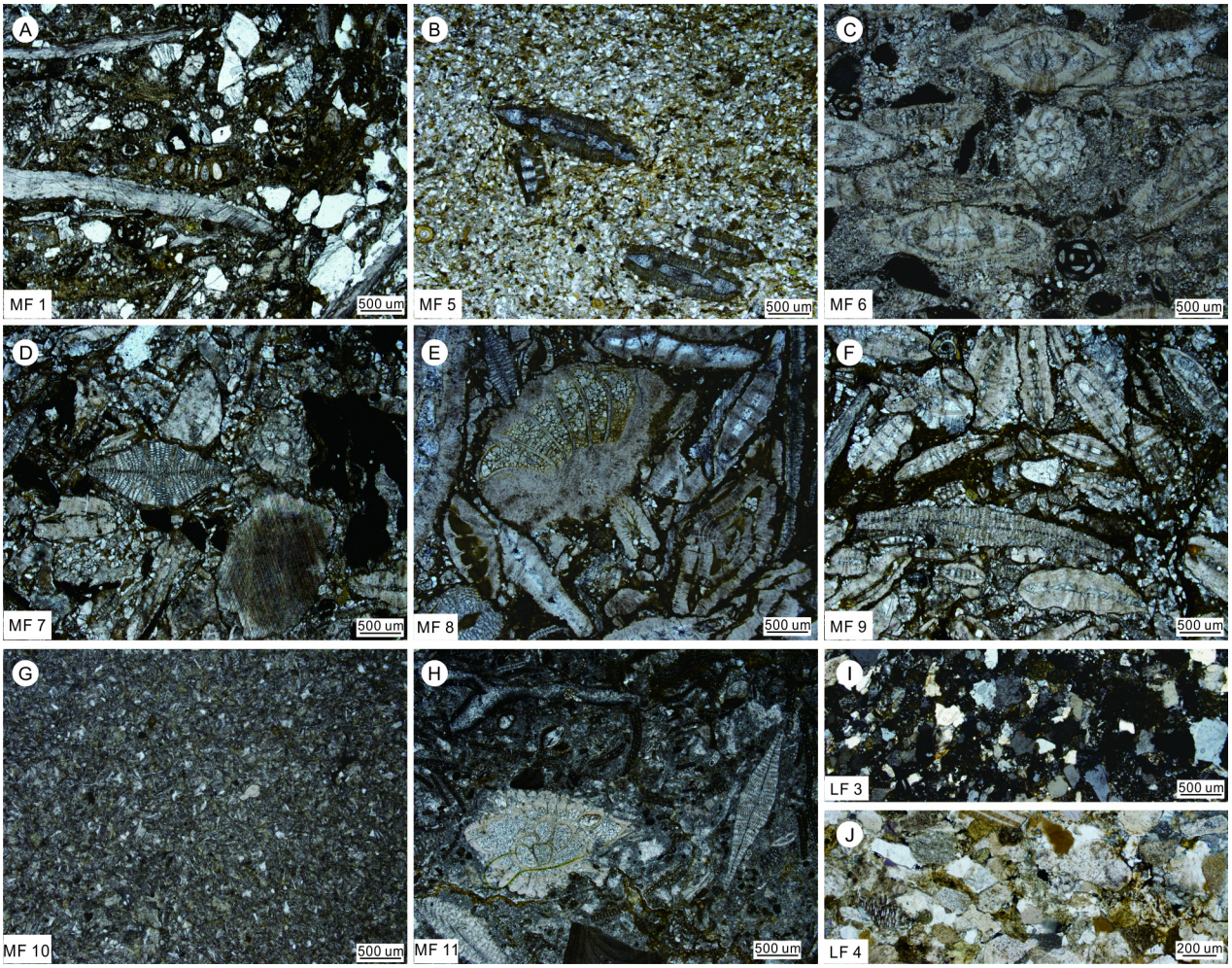

FIGURE 6. Representative microfacies of Jialazi Formation (modified from Jiang *et al*., 2021). **A**, MF1 sandy bioclastic wackestone. **B**, MF5 sandy LBF wackestone. **C**, MF6 sandy *Ranikothalia* floatstone/rudstone. **D**, MF7 bioclastic floatstone/rudstone. **E**, MF8 LBF rudstone. **F**, MF9 LBF rudstone. **G**, MF10 mudstone. **H**, MF11 bioclastic packstone/floatstone. **I**, LF3 feldspatho-lithic sandstone. **J**, LF4 litho-feldspathic sandstone.

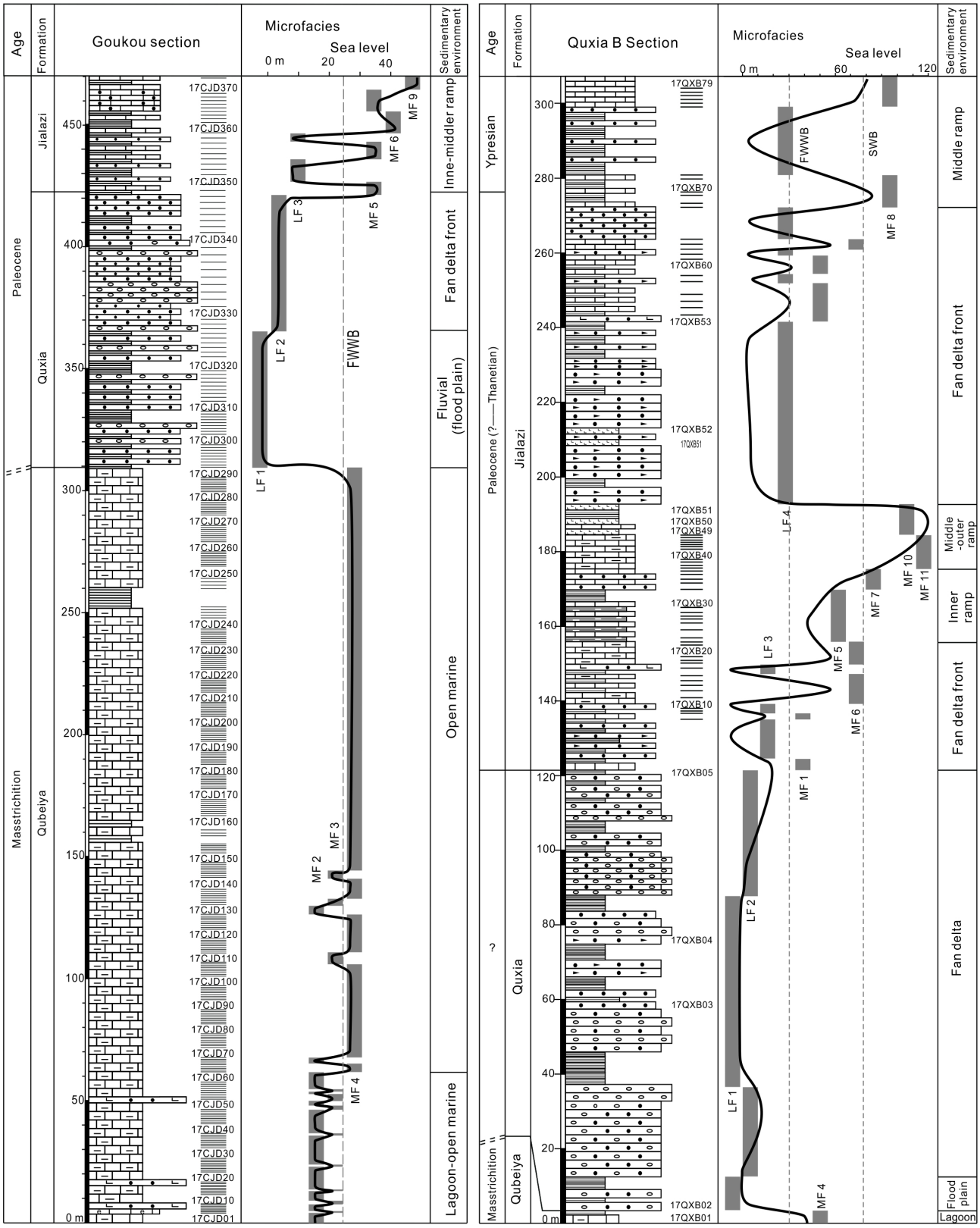

FIGURE 7. Stratigraphic log of Qubeiya, Quxia and Jialazi formations in Goukou and Quxia B sections, showing microfacies, palaeo-water depths, and sedimentary environments. Legend as in Fig. 4. FWWB: fair-weather wave base; SWB: storm wave base.

mudrock and heavily weathered silty sandstones are more erodible and form recesses. LF4 is inferred to testify the rapid progradation of a fan delta, fostered by increasing sediment flux possibly associated with enhanced hydrological cycle in the source area during the PETM event (Jiang *et al*., 2021).

2. Lagoon

In the lower and upper Jialazi Formation, MF1 (sandy bioclastic wackestone) is characterized by abundant fragments of gastropods, bivalves and miliolids (10–30%) with sand-sized terrigenous clasts set in micritic matrix. High-energy transport followed by deposition in a restricted, low-energy shallow-marine environment within the photic zone is indicated (Scholle & Ulmer-Scholle, 2003; Flügel, 2010; Fig. 6A).

3. Open marine

MF5 to MF7 mainly occur in the lower Jialazi Formation. MF5 (sandy wackestone with large benthic foraminifera) is dominated by *Ranikothalia* and *Assilina*, associated with fragments of bryozoans, bivalves, coralline algae, as well as minor miliolids and gastropods (Fig. 6B). MF6 (sandy *Ranikothalia* floatstone/rudstone) also includes mostly well-preserved and elongated *Daviesina* and *Miscellanea*, as well as minor bivalve and echinoderm fragments (Fig. 6C). MF7 (bioclastic floatstone/rudstone) contains foraminifera (*Discocyclina, Assilina*, *Ranikothalia*), bivalves, echinoderms, bryozoans, coralline algae, and a few intraclasts (Fig. 6D).

The diversified biota in MF5–MF7 mostly consists of benthic foraminifera with elongated shapes, suggesting an open and relatively deep-water environment (Geel, 2000; Beavington-Penney & Racey, 2004; Baumgartner-Mora & Baumgartner, 2016). Commonly intact shells and micritic matrix suggest quasi-autochthonous deposition in a low-energy inner ramp. The sand fraction may indicate either terrigenous input or erosion of hard substrates by currents (Flügel, 2010).

4. Middle-outer ramp

Whereas MF8 mainly occurs at the top of the Jialazi Formation, MF9 to MF11 are mostly found at the top of the lower Jialazi Formation. MF8 (LBF rudstone) consists of thick-bedded bioclastic limestone dominated by benthic foraminifera (> 90%), including elongated or oval-shaped *Discocyclina*, *Assilina*, *Nummulites*, and *Operculina*. *Nummulites* typically inhabit clean-water environments at depths of 10-60 m (Beavington-Penney & Racey, 2004), whereas *Discocyclina* and *Assilina* indicate water depths exceeding 80 m (Hottinger, 1997; Geel, 2000). Foraminiferal tests are commonly oriented, suggesting storm influence. MF8 is inferred to represent a middle-ramp between storm and fair-weather wave base.

MF9 (LBF rudstone), mainly represented in thin-bedded limestones, contains abundant *Discocyclina* and *Assilina* (~60%), along with bivalves, coralline algae, echinoderms, and intraclasts (Fig. 6F). The *Discocyclina* - *Assilina* assemblage indicates a deeper-water environment. MF10 is mainly represented in thin-bedded micritic limestone lacking distinct sedimentary structures (Fig. 6G). MF11 (bioclastic packstone/floatstone), represented in the interbedded thick-bedded grey bioclastic limestone, is characterized by coralline algae (*Rodophyte*) associated with the microproblematic fossil *Distichoplaxy*, benthic foraminifera (*Discocyclina*, *Assilina*, *Miscellanea*), and planktonic foraminifera (*Morozovella)* (Fig. 6H).

The semi-oriented stacking of bioclasts and the presence of intraclasts suggest high-energy hydrodynamic conditions on a middle to outer ramp between storm and fair-weather wave base for MF9 as well as for MF11 (Flügel, 2010; Sarkar, 2018). MF10 points to a quieter depositional condition below storm wave base.

Discussion

Sedimentary environmental evolution

High-resolution facies and microfacies analysis documents two regressive-transgressive sequences in the upper Maastrichtian to lower Eocene Cuojiangding succession (Figs 7, 9). The Qubeiya Formation was deposited before the first shoaling event in a relative stable lagoonal-open marine environment with frequent terrigenous influx (MF2-3) and storm influence in the middle-upper part (MF4). The first shoaling event is testified by the Qubeiya/Quxia boundary, when shallow-marine carbonates were replaced by terrestrial floodplain deposits (LF1), passing upward to fan-delta conglomerate-sandstone-claystone cyclothems (LF2) in the upper Quxia Formation and eventually to fan-delta-front sandstone, limestone and claystone (LF3) at the base of the Jialazi Formation.

A gradual transgression is recorded by the lower Jialazi Formation, when carbonate deposition resumed as low-energy restricted-lagoon deposits (MF1), followed by open-marine rudstone with *Ranikothalia* (MF5), wackestone with *Assilina* and *Ranikothalia* (MF6), and floatstone with *Discocyclina*, *Assilina*, and *Ranikothalia* (MF7; Fig. 7). Middle-outer-ramp mudstone and packstone with red algae, rhodophytes, coralline algae, *Distichoplax biserialis*, and large benthic foraminifera (MF9–MF11) indicate that the deepest palaeo-water conditions were reached at the top of the lower Jialazi Formation.

The second shoaling event is marked by the sharp transition to massive siliciclastic rocks (LF4) in the middle Jialazi Formation, followed by a second deepening trend in the upper Jialazi Formation, culminating in the deposition of floatstone (MF8) with abundant foraminifera in a middle-ramp environment.

Control factors of sedimentary evolution

The uppermost Cretaceous to lower Paleogene succession exposed in the Cuojiangding area documents the final stage of the Xigaze forearc basin, with three (Qubeiya,

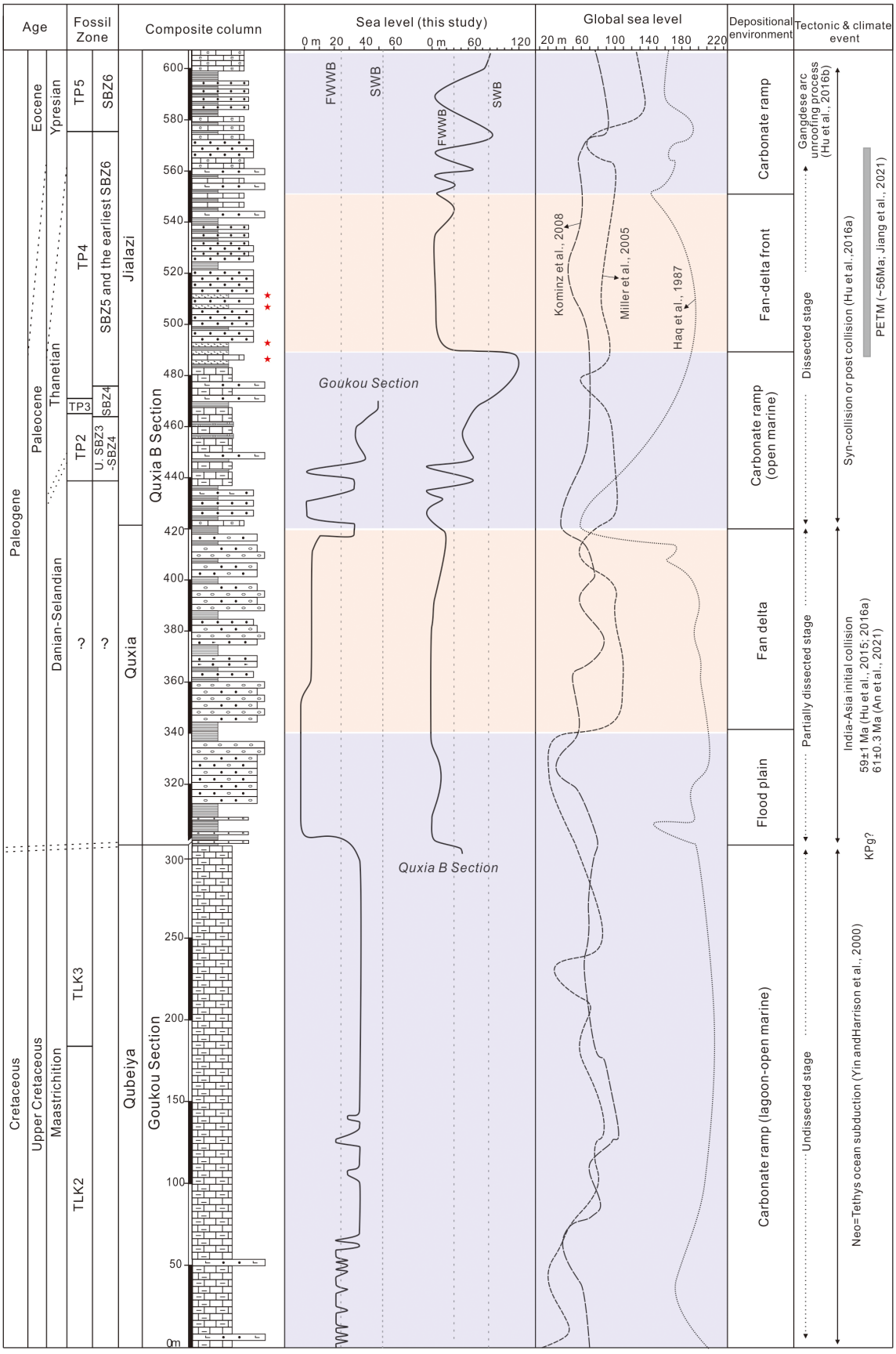

FIGURE 8. Comparison between inferred palaeowater-depth curve for Cuojiangding succession and eustatic curves of Haq *et al*. (1987), Miller *et al*. (2005), and Kominz *et al*. (2008). FWWB: fair-weather wave base; SWB: storm wave base. Highlighted in light greysh blue and light yellow are time intervals when local paleo-water depth and eustatic curves are consistent and inconsistent, respectively. Legend as in Fig. 4.

lower Jialazi, and upper Jialazi) carbonate intervals separated by two (Quxia and middle Jialazi) siliciclastic intervals. A comparison with the most widely used eustatic curves (*i.e*., Haq *et al*., 1987; Miller *et al*., 2005; Kominz *et al*., 2008) sheds further light on the palaeogeodynamic and palaeoenvironmental evolution during this period of fundamental tectonic and climatic change.

The uppermost Cretaceous Qubeiya Formation, conformably overlying the deltaic Padana Formation (Liu *et al*., 1988), mostly consists of shallow-marine marlstone rich in *Lepidorbitoides* (Fig. 9A). It thus documents a marine transgression concordant with relatively high global sea level during this period (Fig. 8). Previous studies have considered the contact between the Qubeiya Formation and the overlying Quxia Formation as unconformable and related to a regional tectonic event (Liu *et al*., 1988; Ding *et al*., 2005; Hu *et al*., 2016b). In the Quxia B section, however, we did not see any major discontinuity between the purplish-red marls at the top of the Qubeiya Formation and a 30-cm-thick gray-green mudrock layer, followed in turn by medium-bedded, medium-grained sandstone at the base of the Quxia Formation (Fig. 2D). Facies analysis suggests that the top of the Qubeiya Formation documents a deep lagoonal to shallow-marine environment, whereas the base of the Quxia Formation represents a floodplain environment (Fig. 9B). This regression may correspond to the eustatic fall at the end of the Maastrichtian (Haq, 1987; Kominz et al., 2008), which could have contributed to the extinction of ammonites (Sun and Wang, 2001) and marine species of benthic foraminifera (BouDagher-Fadel & Price, 2013).

The siliciclastic cyclothems in the middle to upper Quxia Formation indicate a subaerial fan-delta environment (Fig. 9C; Wang *et al*., 2012; Hu *et al*., 2016b). Particularly at a time of high global sea-level, this event can be safely ascribed to active tectonics (Nemec & Steel, 1988). The deposition of the Quxia Formation is constrained between 66 Ma (maximum depositional age based on detrital-zircon chronostratigraphy; Hu *et al*., 2016b) and 56 Ma (U-Pb age of 56.1–55.1 Ma of zircons in tuff layers in the middle Jialazi Formation; Jiang *et al*., 2021). Further constraints are provided by biostratigraphy. *Lepidorbitoides*-dominated foraminiferal assemblages in the Qubeiya Formation correspond to the Maastrichtian *Orbitoides* fauna reported from the Gamba area of the Tethys Himalaya, whereas the *Miscellanea-Daviesina-Ranikothalia* assemblage from the base of the Jialazi Formation corresponds to the upper Paleocene (Selandian-Thanetian) *Miscellanea-Daviesina* fauna (Wan *et al*., 2001, 2002). Chronostratigraphic and biostratigraphic evidence constrains the depositional age of the Quxia Formation as Danian-Selandian (~66–59 Ma), coinciding with the final stage of oceanic Neotethyan subduction and initial continental subduction of India and collision with Asia (Hu *et al*., 2015, 2016a; An *et al*., 2021). Following Hu et al. (2016b), we maintain that the onset of the collision triggered rapid uplift and erosional exhumation of the southern margin of the Gangdese arc, feeding fan-delta deposits of the Quxia Formation into the Xigaze forearc basin (Fig. 9D).

The lower Jialazi Formation documents a transgressive transition from fan-delta-front to carbonate-ramp environments in concordance with a global sea-level rise inferred to have occurred at this time (Fig. 9E). Terrigenous detritus in sandy limestones, still derived from unroofing of the Gangdese arc (Hu *et al*., 2016b), decreases up-section, and larger benthic foraminifera, echinoderms, and bivalves could thus thrive and maintain carbonate production (Wilson & Lokier, 2002). Terrigenous supply sharply increased during deposition of the middle Jialazi Formation, where siliciclastic layers reach thicknesses up to 50 m. The balance of biological production was disrupted, inhibiting the growth of the carbonate factory entirely (Tcherepanov *et al*., 2008) while siliciclastic and volcaniclastic sediments were forcing the coastline to prograde (Fig. 9E). The enhanced hydrological cycle during the PETM may have contributed to the intensification of erosion in the source area (Jiang *et al*., 2021). After the PETM, terrigenous supply decreased, and carbonate-ramp sedimentation resumed at a time of high sea level (Fig.7).

Conclusion

Detailed stratigraphic and palaeontological studies of the Xigaze forearc basin succession exposed in the Cuojiangding area reveal a three-stage evolutionary process from the late Maastrichtian to the early Eocene. The late Maastrichtian Qubeiya Formation, rich in benthic foraminifera, records a deep lagoon to shallow-marine environment with terrigenous input. This is succeeded by a floodplain environment in the lower Quxia Formation, characterized by a thick sequence of purplish-red and gray-green mudrock with interbedded sandstone. Multiple fining-upward cyclothems dominated by coarse siliciclastic deposits document the development of a fan delta in the upper Quxia Formation. The Paleocene-Eocene Jialazi Formation consists of interbedded carbonate, sandstone, and mudrock deposited on a carbonate ramp influenced by terrigenous input.

A comparison with the most widely used eustatic curves highlights alternating phases of tectonic and eustatic control during the latest Cretaceous-early Paleogene residual marine stage of the Xigaze forearc basin. In both Qubeiya and Jialazi formations, transgressive carbonate intervals were deposited during high-stands. The development of the carbonate platform was interrupted

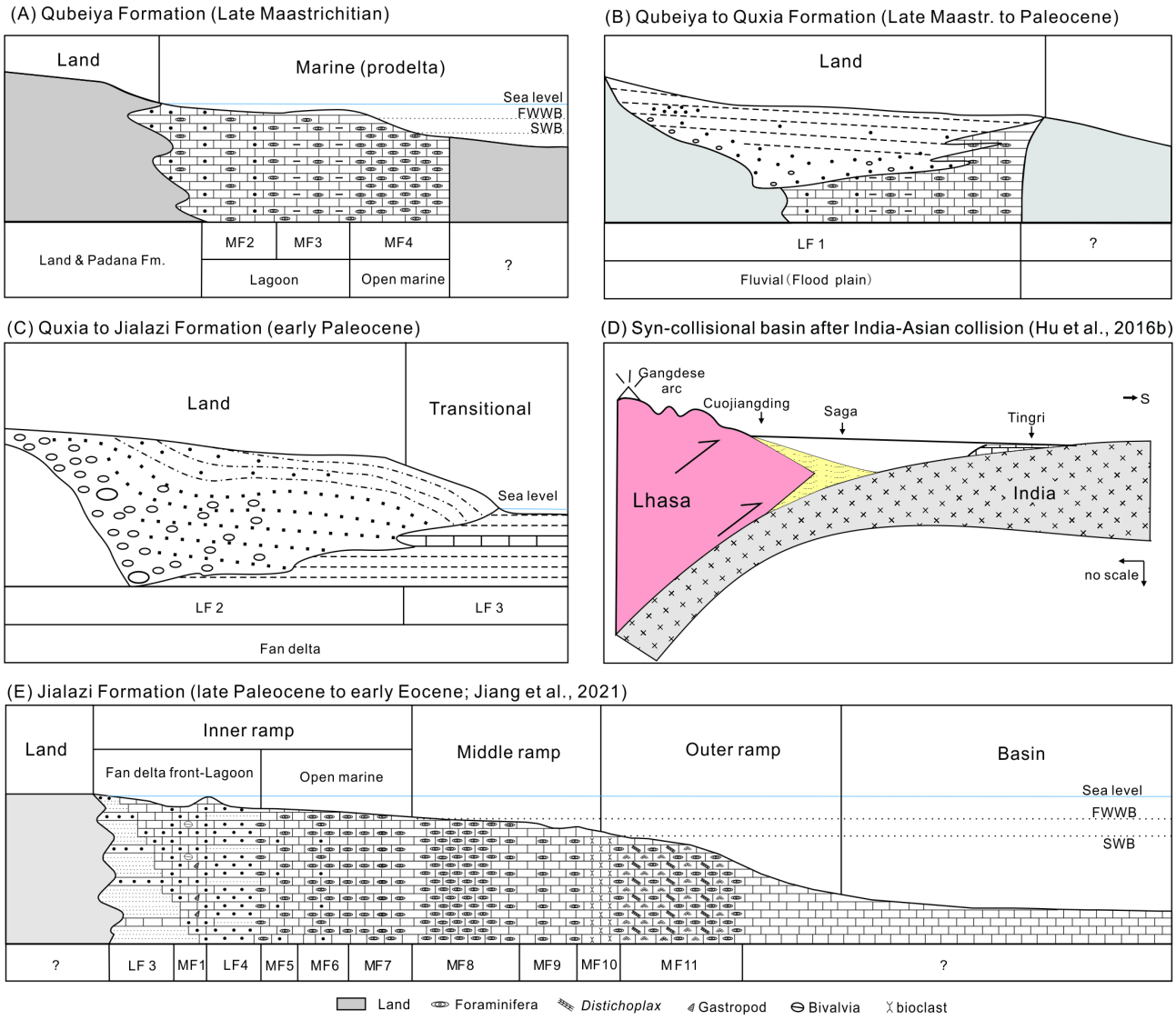

FIGURE 9. Depositional model for upper Maastrichtian to lowermost Eocene strata exposed in Cuojiangding area (**A**–**E**), showing relative position of microfacies (MF) and lithofacies (LF). FWWB: fair-weather wave base; SWB: storm wave base. **D** is modified from Hu *et al*., 2016(b) and **E** is modified from Jiang *et al*. (2021). Legend as in Fig. 4.

by two regressive episodes that both contrast with the global sea-level trends. The first, documented by fan-delta deposits in the Quxia Formation, occurred during the initial subduction of the Indian continental margin beneath Asia and was thus most probably tectonically controlled. The second, recorded by the middle Jialazi Formation, occurred during the PETM, likely driven by an intensified hydrological cycle, suggesting a climatic control.

Acknowledgements

Juan Li, Pu Mi and Hanpu Fu are thanked for assistance in the field. This work was supported by the National Natural Science Foundation of China (42488201, 42402126), and China Postdoctoral Science Foundation (2024M751379), Postdoctoral Fellowship Program of China Postdoctoral Science Foundation (GZC20231096), the Second Tibetan Plateau Scientific Expedition and Research Program (STEP, Grant No. 2019QZKK0204). This is a contribution to the IGCP739. This paper is dedicated to our dear friend Dr Juan Li who spent her last moments logging the PETM interval in the Tibetan Himalaya.

References

An, W., Hu, X., Garzanti, E., BouDagher-Fadel, M.K., Wang, J. & Sun, G. (2014) Xigaze forearc basin revisited (South Tibet): Provenance changes and origin of the Xigaze Ophiolite. *Geological Society of America Bulletin*, 126 (11-12), 1595–

1613.
https://doi.org/10.1130/B31020.1

An, W., Hu, X., Garzanti, E., Wang, J.G. & Liu, Q. (2021) New precise dating of the India-Asia collision in the Tibetan Himalaya at 61 Ma. *Geophysical Research Letters*, 48 (3), e2020GL090641.
https://doi.org/10.1029/2020GL090641

Baumgartner-Mora, C. & Baumgartner, P.O. (2016) Paleocene-earliest Eocene larger benthic foraminifera and Ranikothalia-bearing carbonate paleo-environments of Costa Rica (South Central America). *Micropaleontology*, 62 (6), 453–508.

Beavington-Penney, S.J. & Racey, A. (2004) Ecology of extant nummulitids and other larger benthic foraminifera: applications in palaeo-environmental analysis. *Earth-Science Reviews*, 67, 219–265.
https://doi.org/10.1016/j.earscirev.2004.02.005

BouDagher-Fadel, M.K. (2018) Evolution and geological significance of larger benthic foraminifera. *Second ed. UCL Press, London*, 689 pp.

BouDagher-Fadel, M.K. & Price, G. (2013) The phylogenetic and palaeogeographic evolution of the miogypsinid larger benthic foraminifera. *Journal of the Geological Society*, 170 (1), 185–208.
https://doi.org/10.1144/jgs2011-149

BouDagher-Fadel, M.K., Price, G.D., Hu, X. & Li, J. (2015) Late cretaceous to early Paleogene foraminiferal biozones in the Tibetan Himalayas, and a pan-Tethyan foraminiferal correlation scheme. *Stratigraphy*, 12, 67–91.
https://doi.org/10.29041/strat.12.1.05

Cawood, P.A. (2005) Terra Australis orogen: Rodinia breakup and development of the Pacific and Iapetus margins of Gondwana during the Neoproterozoic and Paleozoic. *Earth-Science Reviews*, 69, 249–279.
https://doi.org/10.1016/j.earscirev.2004.09.001

DeCelles, P.G., Kapp, P., Gehrels, G.E. & Ding, L. (2014) Paleocene Eocene foreland basin evolution in the Himalaya of southern Tibet and Nepal: implications for the age of initial India-Asia collision. *Tectonics*, 33 (5), 824–849.
https://doi.org/10.1002/2014TC003522

DeGraaff-Surpless, K., Graham, S.A., Wooden, J.L. & McWilliams, M.O. (2002) Detrital zircon provenance analysis of the Great Valley Group, California: Evolution of an arc-forearc system: *Geological Society of America Bulletin*, 114 (12), 1564–1580.
https://doi.org/10.1130/0016-7606(2002)114<1564:DZPAOT>2.0.CO;2

Dickinson, W.R. (1995) Forearc basins. *In*: Busby, C.J. & Ingersoll, R.V. (Eds), *Tectonics of sedimentary basins*. Blackwell Science, Cambridge, Massachusetts, pp. 211–261.

Ding, L., Kapp, P. & Wan, X. (2005) Paleocene Eocene record of ophiolite obduction and initial India-Asia collision, south Central Tibet. *Tectonics*, 24, 1–18.
https://doi.org/10.1029/2004TC001729

Ding, L., Qasim, M., Jadoon, I., Khan, M., Xu, Q., Cai, F., Wang, H., Baral, U., Yue, Y. (2016) The India-Asia collision in north Pakistan: Insight from the U-Pb detrital zircon provenance of Cenozoic foreland basin. *Earth and Planetary Science Letter*, 455, 49–61.
https://doi.org/10.1016/j.epsl.2016.09.003

Dunham, R.J. (1962) Classification of carbonate rocks according to deposition texture. *In*: Ham, W.E. (Ed.), Classification of Carbonate Rocks. *American Association of Petroleum Geologists*, 1, 108–121.
https://doi.org/10.1306/M1357

Dürr, S.B. (1996) Provenance of Xigaze forearc basin clastic rocks (Cretaceous, south Tibet). *Geological Society of America Bulletin*, 108 (6), 669–684.
https://doi.org/10.1130/0016-7606(1996)108<0669:POXFAB>2.3.CO;2

Einsele, G., Liu, B., Dürr, S., Frisch, W., Liu, G., Luterbacher, H.P., Ratschbacher, L., Ricken, W., Wendt, J., Wetzel, A., Yu, G. & Zheng, H. (1994) The Xigaze forearc basin: evolution and facies architecture (Cretaceous, Tibet). *Sedimentary Geology*, 90 (1-2), 1–32.
https://doi.org/10.1016/0037-0738(94)90014-0

Embry, A.F. & Klovan, J.E. (1971) A late Devonian reef tract on northeastern Banks Island, NWT. *Bulletin of Canadian Petroleum Geology*, 19 (4), 730–781.
https://doi.org/10.35767/gscpgbull.19.4.730

Flügel, E. (2010) *Microfacies of carbonate rocks: Analysis, interpretation and application*. Springer-Verlag, Berlin Heidelberg, New York, 976 pp.
https://doi.org/10.1007/978-3-642-03796-2

Garzanti, E., Baud, A. & Mascle, G. (1987) Sedimentary record of the northward flight of India and its collision with Eurasia (Ladakh Himalaya, India). *Geodinamica Acta*, 1, 297–312.
https://doi.org/10.1080/09853111.1987.11105147

Garzanti, E. & Van Haver, T. (1988) The Indus clastics: forearc basin sedimentation in the Ladakh Himalaya (India). *Sedimentary Geology*, 59 (3-4), 237–249.
https://doi.org/10.1016/0037-0738(88)90078-4

Geel, T. (2000) Recognition of stratigraphic sequences in carbonate platform and slope deposits: empirical models based on microfacies analysis of Palaeogene deposits in southeastern Spain. *Palaeogeography, Palaeoclimatology, Palaeoecology*, 155, 211–238.
https://doi.org/10.1016/S0031-0182(99)00117-0

Haq, B.U., Hardenbol, J.A.N. & Vail, P.R. (1987) Chronology of fluctuating sea levels since the Triassic. *Science*, 235 (4793), 1156–1167.
https://doi.org/10.1126/science.235.4793.1156

Hottinger, L. (1997) Shallow benthic foraminiferal assemblages as signals for depth of their deposition and their limitations. *Bulletin de la Société géologique de France*, 168 (4), 491–505.

Hu, X., Garzanti, E., Moore, T. & Raffi, I. (2015) Direct stratigraphic dating of India-Asia collision onset at the Selandian (middle

Paleocene, 59 ± 1 Ma). *Geology*, 43, 859–862. https://doi.org/10.1130/G36872.1

Hu, X., Garzanti, E., Wang, J., Huang, W., An, W. & Webb, A. (2016a) The timing of India-Asia collision onset–Facts, theories, controversies. *Earth-Science Reviews*, 160, 264–299. https://doi.org/10.1016/j.earscirev.2016.07.014

Hu, X., Wang, J., BouDagher-Fadel, M., Garzanti, E. & An, W. (2016b) New insights into the timing of the India-Asia collision from the Paleogene Quxia and Jialazi formations of the Xigaze forearc basin, South Tibet. *Gondwana Research*, 32, 76–92. https://doi.org/10.1016/j.gr.2015.02.007

Ingalls, M. (2019) Reconstructing carbonate alteration histories in orogenic sedimentary basins: Xigaze forearc, southern Tibet. *Geochimica et Cosmochimica Acta*, 251, 284–300. https://doi.org/10.1016/j.gca.2019.02.005

Ingersoll, R.V. (1979) Evolution of the Late Cretaceous forearc basin, northern and central California. *Geological Society of America Bulletin*, 90 (9), 813–826. https://doi.org/10.1130/0016-7606(1979)90<813:EOTLCF>2.0.CO;2

Jiang, J., Hu, X., Li, J., BouDagher-Fadel, M. & Garzanti, E. (2021) Discovery of the Paleocene-Eocene Thermal Maximum in shallow-marine sediments of the Xigaze forearc basin, Tibet: A record of enhanced extreme precipitation and siliciclastic sediment flux. *Palaeogeography, Palaeoclimatology, Palaeoecology*, 562, 110095. https://doi.org/10.1016/j.palaeo.2020.110095

Kahsnitz, M.M., Willems, H., Luo, H. & Zhou, Z.C. (2017) Paleocene and lower Eocene shallow-water limestones of Tibet: Microfacies analysis and correlation of the eastern Neo-Tethyan Ocean. *Palaeoworld*, 27, 226–246. https://doi.org/10.1016/j.palwor.2017.12.002

Kominz, M.A., Browning, J.V., Miller, K.G., Sugarman, P.J., Mizintseva, S. & Scotese, C.R. (2008) Late Cretaceous to Miocene sea-level estimates from the New Jersey and Delaware coastal plain coreholes: An error analysis. *Basin Research*, 20 (2), 211–226. https://doi.org/10.1111/j.1365-2117.2008.00354.x

Li, J., Batten, D.J. & Zhang, Y. (2008) Late Cretaceous palynofloras from the southern Laurasian margin in the Xigaze region, Xizang (Tibet). *Cretaceous Research*, 29, 294–300. https://doi.org/10.1016/j.cretres.2007.05.002

Liu, C., Yin, J., Sun, X. & Sun, Y. (1988) Marine Late Cretaceous–early Tertiary sequence-the non-flysch deposits of the Xigaze forearc basin in South Xizang. *Journal of Institute Geology Chinese Academy Sciences*, 3, 130–157. [In Chinese with English abstract]

Malarkodi, N., Özcan, E., Venkataraman, D., Somappa, S.C., Gowda, S., Nagaraja, P.K.T. & Yücel, A.O. (2017) *Lepidorbitoides* (foraminifera) from the lower Maastrichtian Kallankuruchchi Formation, Cauvery Basin, India: morphometry and paleobiogeography. *Cretaceous Research*, 77, 143–157. https://doi.org/10.1016/j.cretres.2017.05.009

McPherson, J.G., Shanmugam, G. & Moiola, R.J. (1987) Fan-deltas and braid deltas: varieties of coarse-grained deltas. *Geological Society of America Bulletin*, 99 (3), 331–340. https://doi.org/10.1130/0016-7606(1987)99<331:FABDVO>2.0.CO;2

Miall, A.D. (2013) *The geology of fluvial deposits: sedimentary facies, basin analysis, and petroleum geology*. Springer, Berlin, 581 pp.

Miller, K.G., Kominz, M.A., Browning, J.V., Wright, J.D., Mountain, G.S., Katz, M.E., Sugarman, P.J., Cramer B.S., Christie-blick, N. & Pekar, S.F. (2005) The Phanerozoic record of global sea-level change. *Science*, 310 (5752), 1293–1298. https://doi.org/10.1126/science.1116412

Mount, J. (1985) Mixed siliciclastic and carbonate sediments: a proposed first-order textural and compositional classification. *Sedimentology*, 32, 435–442. https://doi.org/10.1111/j.1365-3091.1985.tb00522.x

Nemec, W. & Steel, R.J. (1988) What is a fan delta and how do we recognize it? *Fan Deltas: sedimentology and tectonic settings*, 3, 231–248.

Orme, D.A., Carrapa, B. & Kapp, P. (2015) Sedimentology, provenance and geochronology of the upper Cretaceous–lower Eocene western Xigaze forearc basin, southern Tibet. *Basin Research*, 27 (4), 387–411. https://doi.org/10.1111/bre.12080

Qian, D., Zhang, S. & Gu, Q. (1982) Some new data on the age of the Ngamring formation of the Xigaze Group in southern Xizang (Tibet). *China. Scientia Geologica Sinica*, 3, 329–332. [In Chinese with English abstract]

Robles-Salcedo, R., Rivas, G., Vicedo, V. & Caus, E. (2013) Paleoenvironmental distribution of larger foraminifera in Upper Cretaceous siliciclastic-carbonate deposits (Arén Sandstone Formation, South Pyrenees, northeastern Spain). *Palaios*, 28 (9), 637–648. https://doi.org/10.2110/palo.2012.p12-125r

Sarkar, S. (2018) The enigmatic Palaeocene-Eocene coralline *Distichoplax*: Approaching the structural complexities, ecological affinities and extinction hypotheses. *Marine Micropaleontology*, 139, 72–83. https://doi.org/10.1016/j.marmicro.2017.12.001

Scholle, P.A. & Ulmer-Scholle, D.S. (2003) A color guide to the petrography of carbonate rocks: grains, textures, porosity, diagenesis. *American Association of Petroleum Geologists, Tulsa, AAPG Memoir*, 77, 474 pp. https://doi.org/10.1306/M77973

Serra-Kiel, J., Hottinger, L., Caus, E., Drobne, K., Ferrandez, C., Jauhri, A.K., Less, G., Pavlovec, R., Pignatti, J., Samso, M.J., Schaub, H., Sirel, E., Strougo, A., Tambaregu, Y., Tosquella, J. & Zakrevskaya, E. (1998) Larger foraminifera biostratigraphy of the Tethyan Paleocene and Eocene. *Bulletin de la Société géologique de France*, 169, 281–299.

Sun, Y.Y. & Wang, Y.G. (2001) Late Campanian to early Maastrichtian ammonoid fauna of Late Cretaceous in Xizang the youngest ammonoid fauna in China. *Acta Palaeontologica Sinica*, 40, 20–30. [In Chinese with English abstract]

Tcherepanov, E.N., Droxler, A.W., Lapointe, P., Dickens, G.R., Bentley, S.J., Beaufort, L., Peterson, L.C., Daniell, J. & Opdyke, B.N. (2008) Neogene evolution of the mixed carbonate-siliciclastic system in the Gulf of Papua, Papua New Guinea. *Journal of Geophysical Research: Earth Surface*, 113 (F1). https://doi.org/10.1029/2006JF000684

Wan, X., Ding, L., Li, J. & Cai, H. (2001) Latest Cretaceous to early Eocene marine strata in the Zhongba region, Tibet. *Journal of Stratigraphy* 25, 267–272. [In Chinese with English abstract]

Wan, X., Jansa, L. F., & Sarti, M. (2002) Cretaceous and Paleogene boundary strata in southern Tibet and their implication for the Indi-Eurasia collision. *Lethaia*, 35 (2), 131–146. https://doi.org/10.1111/j.1502-3931.2002.tb00074.x

Wan, X., Luo, W., Wang, C.S. & Luba, J.S. (1998) Discovery and significance of Cretaceous fossils from the Xigaze forearc basin, Tibet. *Journal of Asian Earth Sciences*, 16, 217–223. https://doi.org/10.1016/S0743-9547(98)00012-9

Wang, C., Liu, Z., Li, X. & Wan, X. (1999) *Xigaze forearc basin and Tsangpo Suture Zone, Tibet*. Geological Publishing House, Beijing, 237 pp. [In Chinese]

Wang, C., Li, X., Liu, Z., Li, Y., Jansa, L., Dai, J. & Wei, Y. (2012) Revision of the Cretaceous–Paleogene stratigraphic framework, facies architecture and provenance of the Xigaze forearc basin along the Yarlung Zangbo suture zone. *Gondwana Research*, 22 (2), 415–433. https://doi.org/10.1016/j.gr.2011.09.014

Wang, J., Hu, X., Garzanti, E., An, W. & Liu, X.C. (2017) The birth of the Xigaze forearc basin in southern Tibet. *Earth and Planetary Science Letter*, 465, 38–47. https://doi.org/10.1016/j.epsl.2017.02.036

Wilson, M.E. & Lokier, S.W. (2002) Siliciclastic and volcaniclastic influences on equatorial carbonates: insights from the Neogene of Indonesia. *Sedimentology*, 49 (3), 583–601. https://doi.org/10.1046/j.1365-3091.2002.00463.x

Wu, F.Y., Ji, W.Q., Liu, C.Z. & Chung, S.L. (2010) Detrital zircon U-Pb and Hf isotopic data from the Xigaze fore-arc basin: Constraints on Transhimalayan magmatic evolution in southern Tibet. *Chemical Geology*, 271 (1-2), 13–25. https://doi.org/10.1016/j.chemgeo.2009.12.007